Draft version February 22, 2017
Preprint typeset using LaTeX style emulateapj v. 12/16/11

PROXIMA CENTAURI B WATER LOSS

Rodrigo Luger

1. INTRO

We perform a suite of Markov Chain Monte Carlo (MCMC) runs to obtain constraints on the present-day water content of Proxima Centauri b using the Python code package `emcee` (Foreman-Mackey et al. 2013). MCMC allows one to sample from multi-dimensional probability distributions that are difficult or impossible to obtain directly, which is the case for the ensemble of parameters that control the evolution of the planet surface water content in `VPLANET`. In this section, we develop a framework for inferring the probability distributions of these parameters conditioned on empirical data and our understanding of the physical processes at play.

The input parameters to our model make up the state vector $\mathbf{x}$:

$$\mathbf{x} = \{f_{\rm sat}, t_{\rm sat}, \beta_{\rm xuv}, M_\star, t_\star, a, m\}, \tag{1}$$

corresponding, respectively, to the stellar mass, the XUV saturation fraction, the XUV saturation timescale, the XUV power law exponent, the stellar age, the semi-major axis of the planet, and the mass of the planet. Given a value of $\mathbf{x}$, `VPLANET` computes the evolution of the system from time $t = 0$ to $t = t_\star$, yielding the output vector $\mathbf{y}$:

$$\mathbf{y}(\mathbf{x}) = \{L_\star, L_{\rm xuv}, t_{\rm RG}, m_{\rm H}, m_{\rm H_2O}, P_{\rm O_2}\}, \tag{2}$$

corresponding, respectively, to the stellar luminosity, the stellar XUV luminosity, the duration of the runaway greenhouse phase, the mass of the planet's hydrogen envelope, the mass of water remaining on its surface, and the amount of oxygen (expressed as a partial pressure) retained in either the atmosphere or the surface/mantle, all of which are evaluated at $t = t_\star$ (i.e., the present day). Additional parameters that control the evolution of the planet (initial water content, XUV absorption efficiency, etc.) are held fixed in individual runs; see below.

Our goal in this section is to derive posterior distributions for $\mathbf{y}$ (and in particular for $m_{\rm H_2O}$) given prior information on both $\mathbf{x}$ and $\mathbf{y}$. Some parameters—such as the present-day stellar luminosity—are well-constrained, while others are less well-known and will thus be informed primarily by our choice of prior. This is the case for the XUV saturation fraction, saturation timescale, and power law exponent, which have been studied in detail for solar-like stars (Ribas et al. 2005) but are poorly constrained for M dwarfs. Include some more citations and discuss this a little more... We therefore use flat-log priors for the saturation fraction and timescale, enforcing $-5 \leq \log(f_{\rm sat}) \leq -2$ and $-0.3 \leq \log(t_{\rm sat}/{\rm Gyr}) \leq 1$. We use a Gaussian prior for the XUV power law exponent, with a mean of 1.23, the value derived by (Ribas et al. 2005) for solar-like stars: $\beta_{\rm xuv} \sim \mathcal{N}(-1.23, 0.1)$. We choose an ad hoc standard deviation $\sigma = 0.1$ and verify *a posteriori* that our results are not sensitive to this choice. As we show below, $\beta_{\rm xuv}$ does not strongly correlate with the total water lost or total amount of oxygen that builds up on the planet.

We also use a flat prior for the stellar mass ($0.1 \leq M_\star/{\rm M}_\oplus \leq 0.15$). Although stronger constraints on the stellar mass exist (cite), these are derived indirectly from mass-luminosity relations; we thus enforce a prior on the present-day luminosity to constrain the value of $M_\star$ via our stellar evolution model (see below). We enforce a Gaussian prior on the stellar age $t_\star \sim \mathcal{N}(4.8, 1.4^2)$ Gyr based on the constraints discussed in §(cite).

Our prior on the semi-major axis a is a combination of a Gaussian prior on the orbital period, $P \sim \mathcal{N}(11.186, 0.002^2)$ days (Anglada-Escudé et al. 2016), and the stellar mass prior. Finally, our prior on the planet mass m combines the empirical minimum mass distribution, $m \sin i \sim \mathcal{N}(1.27, 0.18^2)$ ${\rm M}_\oplus$ (Anglada-Escudé et al. 2016), and the a priori inclination distribution for randomly aligned orbits, $\sin i \sim \mathcal{U}(0, 1)$, where $\mathcal{U}$ is a uniform distribution (e.g., Luger et al. 2016).

We further condition our model on measured values of the stellar luminosity $L_\star$ and stellar XUV luminosity $L_{\rm xuv}$. We take $L_\star \sim \mathcal{N}(1.65, 0.15) \times 10^{-3}$ ${\rm L}_\odot$ (Demory et al. 2009) and $\log L_{\rm xuv} \sim \mathcal{N}(-6.36, 0.3^2)$. We base the latter on Ribas et al. (2016), who compiled a comprehensive list of measurements of the emission of Proxima Centauri in the wavelength range 0.6–118 nm. Summing the fluxes over this range and neglecting the contribution of flares, we obtain an XUV flux at Proxima Centauri b $F_{\rm xuv} \approx 252$ erg cm^{-2} s^{-1}, corresponding to $\log L_{\rm xuv} = -6.36$ for $a = 0.0485$ AU. Given the lack of uncertainties for many of the values compiled in Ribas et al. (2016) and the fact that some of those estimates are model extrapolations, it is difficult to establish a reliable error estimate for this value. We make the ad hoc but conservative choice $\sigma = 0.3$ dex, noting that the three measurements that inform the X-ray luminosity of the star in Ribas et al. (2016) (which dominates its XUV emission) have a spread corresponding to $\sigma = 0.2$ dex. However, more rigorous constraints on the XUV emission of Proxima Cen with reliable uncertainties are direly needed to obtain more reliable estimates of water loss from Proxima Cen b.

Given these constraints, we wish to find the posterior distribution of each of the parameters in Equations (1) and (2). We thus define our likelihood function $\mathcal{L}$ for a given state vector $\mathbf{x}$ as

$$\ln \mathcal{L}(\mathbf{x}) = -\frac{1}{2}\left[\frac{(L_\star(\mathbf{x}) - L_\star)^2}{\sigma_{L_\star}^2} - \frac{(L_{\rm xuv}(\mathbf{x}) - L_{\rm xuv})^2}{\sigma_{L_{\rm xuv}}^2}\right] + \ln {\rm Prior}(\mathbf{x}) + C, \tag{3}$$

where $L_\star(\mathbf{x})$ and $L_{\rm xuv}(\mathbf{x})$ are, respectively, the model predictions for the present-day stellar luminosity and stellar XUV luminosity given the state vector $\mathbf{x}$, $L_\star$ and $L_{\rm xuv}$ are their respective observed values, and $\sigma_{L_\star}^2$ and

$\sigma^2_{L_{\rm xuv}}$ are the uncertainties on those observations. The $\ln \text{Prior}(\mathbf{x})$ term is the prior probability and C is an arbitrary normalization constant. Expressed in this form, the observed values of $L_\star$ and $L_{\rm xuv}$ are our "data," while the constraints on the other parameters are "priors," though the distinction is purely semantic.

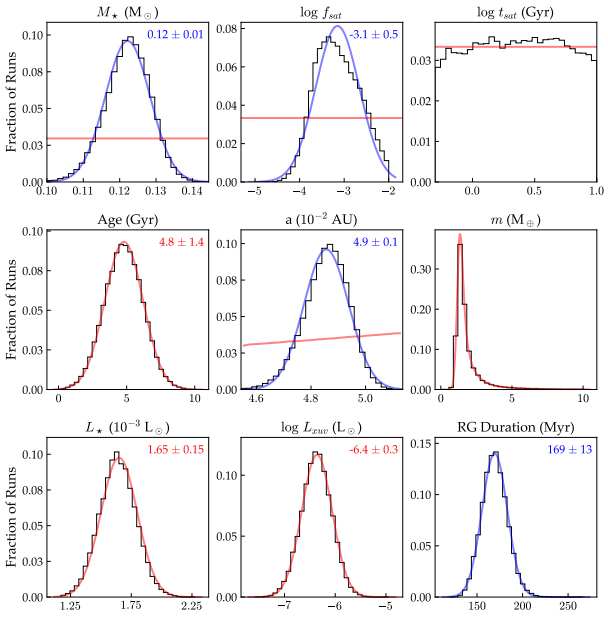

FIG. 1.— Posterior distributions for the various stellar parameters used in the model. The first eight parameters are model inputs, with their corresponding priors shown in red. The combination of these priors and the physical models in `VPLANET` constrain the stellar and planetary parameters shown in this section. Blue curves show Gaussian fits to the posterior distributions, with the mean and standard deviation indicated at the top right. The last panel shows the duration of the runaway greenhouse phase for Proxima Centauri b, one of the model outputs, which we find to be 169 ± 13 Myr.

Given this likelihood function, we use MCMC to obtain the posterior probability distributions for each of the parameters of interest. We draw each of the $\mathbf{x}$ from their respective prior distributions and run 40 parallel chains of 5,000 steps each, discarding the first 500 steps as burn-in. The marginalized posterior distributions for the stellar mass, saturation fraction, saturation timescale, age, semi-major axis, planet mass, present-day stellar luminosity, present-day stellar XUV luminosity, and duration of the runaway greenhouse are shown in Figure 1 as the black histograms. The red curves indicate our priors/data, and the purple curve is a Gaussian fit to the runaway greenhouse duration posterior, yielding $t_{\rm RG} = 169 \pm 13$ Myr.

By construction, the planet mass, stellar age, present-day stellar luminosity, and present-day stellar XUV luminosity posteriors reflect their prior distributions. As mentioned above, the stellar mass posterior is entirely informed by the luminosity posterior via the Spada et al. (2013) stellar evolution tracks. The stellar mass in turn constrains the semi-major axis (via the prior on the period and Kepler's laws). The XUV saturation fraction is fairly well constrained by the present-day XUV luminosity; a log-normal fit to its posterior yields $\log\ f_{\rm sat} = -3.1 \pm 0.5$, which is fully consistent with the observation that M dwarfs saturate at or below $\log\ f_{\rm sat} \approx -3$ (cite). The longer tail at high $f_{\rm sat}$ results from the fact that this parameter is strongly correlated with the saturation timescale, $t_{\rm sat}$ (see Figure 6 below). If saturation is short-lived, the initial saturation fraction must be higher to match the present-day XUV luminosity. Interestingly, our runs do not provide any constraints on $t_{\rm sat}$, whose value is equally likely (in log space) across the range $[0.5, 10]$ Gyr. Finally, the posterior for the XUV power law exponent $\beta_{\rm xuv}$ (not shown in the Figure) is the same as the adopted prior, as the present data is insufficient to constrain it.

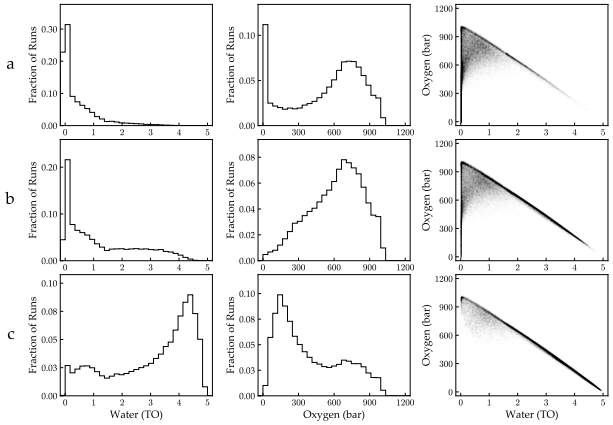

FIG. 2.— Marginalized posteriors for the present-day water content (left) and atmospheric oxygen pressure (center) on Proxima Cen b. The joint posteriors for these two parameters are shown at the right. **(a)** Posteriors for the default run ($m^0_{\rm H_2O} = 5$ TO, $m^0_{\rm H} = 0$, $\epsilon_{\rm xuv} = 0.15$, $\zeta_{\rm O_2} = 0$). **(b)** Same as (a), but for $\epsilon_{\rm xuv} = 0.05$. **(c)** Same as (a), but for $\epsilon_{\rm xuv} = 0.01$. For $\epsilon_{\rm xuv} \gtrsim 0.05$, the planet is desiccated or almost desiccated and builds up between 500 and 900 bars of O_2 in most runs. For $\epsilon_{\rm xuv} \sim 0.01$, the planet loses less water and builds up less O_2, though the loss of more than 1 TO is still likely.

The two quantities that are of the most interest to us — the final water content $m_{\rm H_2O}$ and final O_2 atmospheric pressure $P_{\rm O_2}$ of Proxima Cen b — depend on four additional parameters we must specify: the initial water content $m^0_{\rm H_2O}$, the initial hydrogen mass $m^0_{\rm H}$ (if the planet formed with a primordial envelope), the XUV escape efficiency $\epsilon_{\rm xuv}$, and the O_2 uptake efficiency $\zeta_{\rm O_2}$ of the planet surface. In principle, planet formation models could provide priors on $m^0_{\rm H_2O}$ and $m^0_{\rm H}$, but such models depend on additional parameters that are unknown or poorly constrained. The same is true for the XUV escape efficiency, which can be modeled as in Ribas et al. (2016), and the rate of absorption of O_2 at the surface, which can be computed as in Schaefer et al. (2016). However, given the large number of unknown parameters needed to constrain these four parameters, for simplicity we perform independent MCMC runs for fixed combinations of these. By doing this, we circumvent potential biases arising from incorrect priors on these parameters while still highlighting how our results scale for different assumptions about their values.

In the runs discussed below, our default values are $m^0_{\rm H_2O} = 5$ TO, $m^0_{\rm H} = 0$ $M_\oplus$, $\epsilon_{\rm xuv} = 0.15$, and $\zeta_{\rm O_2} = 0$,

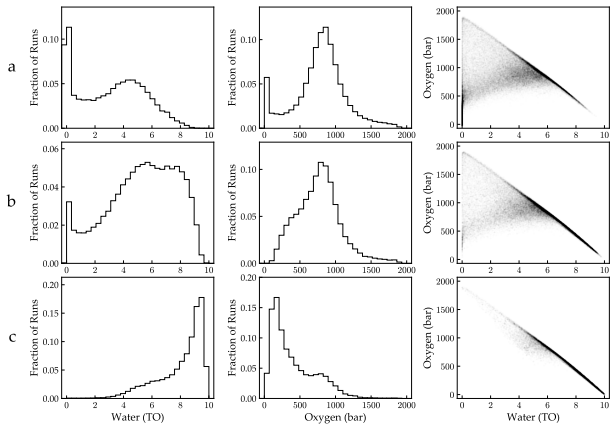

FIG. 3.— Similar to Figure 2, but for an initial water content $m^0_{H_2O} = 10$ TO. As before, the rows correspond to XUV escape efficiencies of 0.15, 0.05, and 0.01 from top to bottom, respectively. For high XUV efficiency, Proxima Cen b loses more than 5 TO in most runs (and is desiccated in $\sim 20\%$ of runs). At lower efficiency, the planet loses less water. The amount of O_2 that builds up is similar to before, but a buildup of more than 1000 bars is now possible.

and we vary each of these parameters in turn. Figure 2 shows the marginalized posterior distributions for the present-day water content (left column) and present-day O_2 atmospheric pressure (middle column), as well as a joint posterior for the two parameters (right column) for three different values of ϵ_{xuv}: **(a)** 0.15, **(b)** 0.05, and **(c)** 0.01. In the first two cases, the planet loses all or nearly all of the 5 TO it formed with, building up several hundred bars of O_2 (with distributions peaking at about 700 bars and with a spread of several hundred bars). For $\epsilon_{xuv} = 0.15$, about 10% of runs result in no substantial oxygen remaining in the atmosphere; in these runs, the escape was so efficient as to remove all of the O_2 along with the escaping H. In the final case, the amount of water lost is significantly smaller: about 2 TO on average, with a peak in the distribution corresponding to a loss of about 0.8 TO. The amount of O_2 remaining is similarly smaller, but still exceeding 100 bars and with similar spread as before. Finally, the joint posterior plots emphasize how correlated the present-day water and oxygen content of Proxima Cen b are. Since the rate at which oxygen builds up in the atmosphere is initially constant at first (**?**), and since the amount of water lost scales with the duration of the escape period, there is a tight linear correlation between the two quantities (lower right hand corner of the joint posterior plots). However, as the atmospheric mixing ratio of oxygen increases, the rate at which hydrogen escapes—and thus the rate at which oxygen is produced—begins to decrease, leading to a break in the linear relationship once $\sim$ 600–700 bars of oxygen build up and leading to the peak in the O_2 posteriors at around that value.

Figure 3 is similar to Figure 2, but shows runs assuming Proxima Cen b formed with 10 TO of water. As before, the rows correspond to different escape efficiencies (0.15, 0.05, 0.01, from top to bottom). The amount of water lost increases in all cases, and for $\epsilon_{xuv} = 0.15$ the planet is desiccated or almost desiccated in about 20% of runs. The amount of O_2 that builds up is similar to that in the previous figure, but O_2 pressures exceeding 1000 bars are now possible in 20–30% of cases for XUV efficiencies of 0.15 or 0.05.

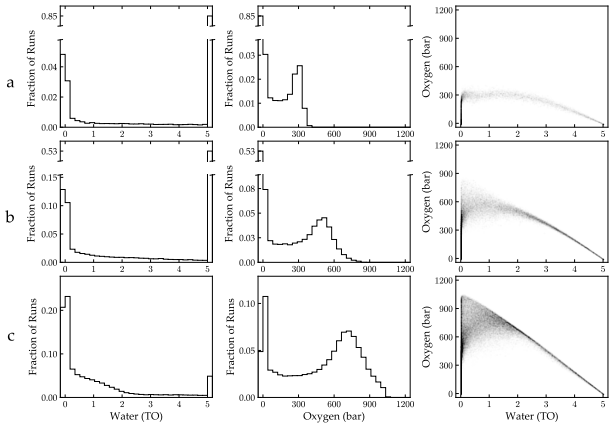

FIG. 4.— Similar to Figure 2, but this time varying the initial mass of the primordial hydrogen envelope of Proxima Cen b. Other parameters are set to their default values. The initial mass of hydrogen is $m^0_H =$ **(a)** 0.01 $M_\oplus$, **(a)** 0.001 $M_\oplus$, and **(a)** 0.0001 $M_\oplus$. Note the broken axes in the first two rows. In the first two cases, no water is lost in more than half of the runs; in such cases, a thin hydrogen envelope remains today. In the final case, most planets lost all their hydrogen and all their water. In order to prevent the runaway loss of its water, Proxima Cen b must have formed with more than 0.01% of its mass in the form of a hydrogen envelope.

In Figure 4 we explore the effect of varying the initial hydrogen content of the planet. From top to bottom, the rows correspond to initial hydrogen masses equal to 0.01, 0.001, and 0.0001 $M_\oplus$. In the first two cases, the effect of the envelope is clear, as most planets lose no water and build up no oxygen. These are mostly cases in which a portion of the hydrogen envelope remains at the present day. However, if the initial hydrogen mass is on the order of 0.0001 $M_\oplus$ (corresponding to roughly 100 times Earth's total atmospheric mass), the shielding effect of the envelope is almost negligible; compare panel **(c)** to the top panel in Figure 2 (the default run). In this case, most of the water is lost to space in the majority of the runs.

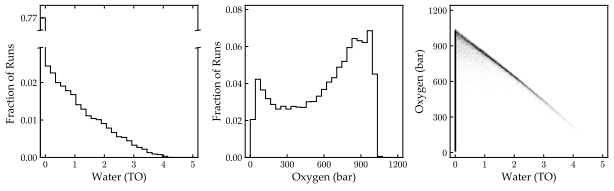

FIG. 5.— The same as panel (a) in Figure 2, but for efficient surface sinks ($\zeta_{O_2} = 1$). The O_2 posterior now corresponds to the amount of oxygen (in bars) absorbed at the planet surface. The absence of atmospheric O_2 facilitates the loss of hydrogen, which must no longer diffuse through the O_2 to escape. In this case, nearly 80% of runs result in complete desiccation (note the broken axis in the first panel). In all cases, Proxima Cen b loses at least 1 TO.

In Figure 5 we show the posteriors assuming the O_2 uptake efficiency of the surface $\zeta_{O_2} = 1$, corresponding to instant O_2 removal by the surface. Compare to the top panel of Figure 2. In this case, the O_2 posterior corresponds to the total amount of oxygen absorbed by the

surface, expressed in bars. While the total amount of oxygen retained by the planet is similar, the fraction of runs in which the planet loses all of its water increases from ~ 20 to ~ 80. This occurs because the buildup of atmospheric O_2 throttles the escape of hydrogen by decreasing its mixing ratio in the upper atmosphere; when O_2 is quickly absorbed at the surface, hydrogen can escape more easily.

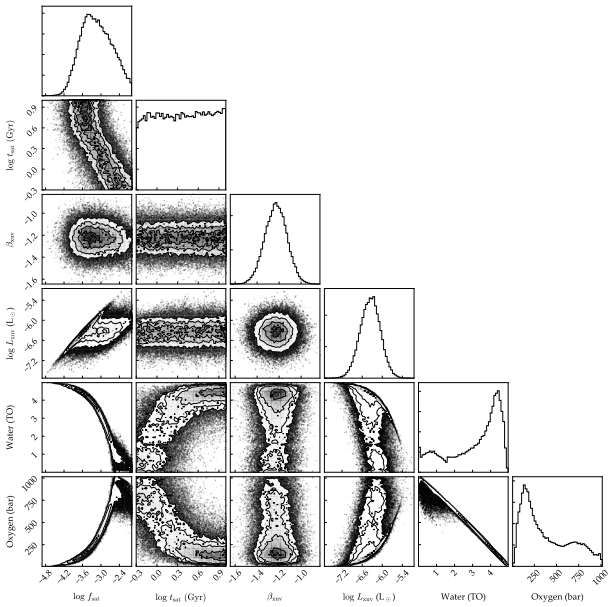

FIG. 6.— Joint posteriors of selected parameters for a run with $\epsilon_{xuv} = 0.01$ [same as Figure 2(c)]. In addition to the correlation between the amount of water lost and the amount of O_2 that builds up, several strong correlations stand out. The strongest ones are between the XUV saturation fraction f_{sat} and the water content (negative) and O_2 pressure (positive). Since most of the water loss occurs in the first few 100 Myr, the value of f_{sat} is the single most important parameter controlling the present-day water and O_2 content of Proxima Cen b. The saturation timescale also correlates with the water and oxygen, but not as strongly; for $t_{sat} \gtrsim 2$ Gyr, its exact value does not significantly affect the evolution of the planet. Shorter saturation timescales correlate with higher saturation fractions and therefore indirectly affect the evolution. Interestingly, the correlation between the XUV power law slope β_{xuv} and the water or O_2 content is negligible, since once saturation ends the water loss rate plummets — the final water content depends almost entirely on the properties of the star early on.

Finally, it is interesting to explore the various correlations between the parameters of the model. It is clear from the previous figures that the amount of oxygen that builds up strongly correlates with the amount of water lost from the planet, but additional correlations exist. In Figure 6 we plot the joint posteriors for the XUV saturation fraction, XUV saturation timescale, XUV power law exponent, present-day XUV luminosity, present-day water content, and present-day O_2 content for a run with $m^0_{H_2O} = 5$ TO, $m^0_H = 0$, $\epsilon_{xuv} = 0.01$, and $\zeta_{O_2} = 0$. The marginalized posteriors are shown at the top. The strongest correlations are between the final water and O_2 contents and the XUV saturation fraction (first column, bottom two panels). The higher the XUV saturation fraction, the more water is lost and the more O_2 builds up. While this may be unsurprising, neither the saturation timescale (second column) nor the power law exponent (third column) correlate as strongly with the water and O_2 content. For saturation timescales longer than about 2 Gyr, the exact duration of the saturation phase does not affect the evolution of the planet, since nearly all of the water loss occurs in the first few 100 Myr. For the same reason, the value of the power law exponent does not significantly correlate with the water or oxygen. On the other hand, the present-day XUV luminosity does correlate with water loss, as it implies a higher XUV luminosity at early times. An accurate determination of f_{sat} and more precise measurements of L_{xuv} are therefore critical to determining the evolution of the water content of Proxima Cen b.

REFERENCES

Anglada-Escudé, G., Amado, P. J., Barnes, J., Berdiñas, Z. M., Butler, R. P., Coleman, G. A. L., de La Cueva, I., Dreizler, S., Endl, M., Giesers, B., Jeffers, S. V., Jenkins, J. S., Jones, H. R. A., Kiraga, M., Kürster, M., López-González, M. J., Marvin, C. J., Morales, N., Morin, J., Nelson, R. P., Ortiz, J. L., Ofir, A., Paardekooper, S.-J., Reiners, A., Rodríguez, E., Rodríguez-López, C., Sarmiento, L. F., Strachan, J. P., Tsapras, Y., Tuomi, M., & Zechmeister, M. 2016, Nature, 536, 437

Demory, B.-O., Ségransan, D., Forveille, T., Queloz, D., Beuzit, J.-L., Delfosse, X., di Folco, E., Kervella, P., Le Bouquin, J.-B., Perrier, C., Benisty, M., Duvert, G., Hofmann, K.-H., Lopez, B., & Petrov, R. 2009, A&A, 505, 205

Foreman-Mackey, D., Hogg, D. W., Lang, D., & Goodman, J. 2013, PASP, 125, 306

Luger, R., Lustig-Yaeger, J., Fleming, D. P., Tilley, M. A., Agol, E., Meadows, V. S., Deitrick, R., & Barnes, R. 2016, ArXiv e-prints

Ribas, I., Bolmont, E., Selsis, F., Reiners, A., Leconte, J., Raymond, S. N., Engle, S. G., Guinan, E. F., Morin, J., Turbet, M., Forget, F., & Anglada-Escudé, G. 2016, A&A, 596, A111

Ribas, I., Guinan, E. F., Güdel, M., & Audard, M. 2005, Astrophys. J., 622, 680

Schaefer, L., Wordsworth, R. D., Berta-Thompson, Z., & Sasselov, D. 2016, ApJ, 829, 63

Spada, F., Demarque, P., Kim, Y.-C., & Sills, A. 2013, ApJ, 776, 87